

## Registration of Temporal Sequences of Coronal and Sagittal Images Obtained from Magnetic Resonance

**Neylor Stevo**, neylorstevo@gmail.com

**Ralf Campos**, ralf.campos@gmail.com

**Renato Seiji Tavares**, reseta@uol.com.br

**Marcos de Sales Guerra Tsuzuki**, mtsuzuki@usp.br

Escola Politécnica da Universidade de São Paulo

**Toshiyuki Gotoh**, gotoh@sci.ynu.ac.jp

**Seiichiro Kagei**, kagei@ynu.ac.jp

Yokohama National University

**Tae Iwasawa**

Kanagawa Cardiovascular and Respiratory Centre

**Abstract.** *It is not possible to see the real movements of the lung, and its visualization, in motion, is an actual topic of research in medicine. There are only two indirect methods to observe the lung in motion: CT (Computerized Tomography) and MRI (Magnetic Resonance Imaging). Methods using MRI are preferable because they do not involve radiation. However, MRI requires longer acquisition times and it is not possible to obtain instantaneous 3D images of the lung through it. As coronal and sagittal sequences of images are orthogonal to each other, their intersection corresponds to a segment in the three dimensional space. The determination of such segment is very important for the registration. For each image in a coronal and a sagittal sequences, the information contained in the intersection segment is determined, and the matching is done to determine the best sagittal images for each coronal image and vice-versa. The lung is an organ that does not have a periodical movement, but a motion that is similar to that of inflation and disinflation of a balloon. The registration is the determination of the best images in a sequence that fits a chosen image in another sequence. The exact instant might not be possible to be determined, as time and space were discretized by the MRI. The registration will be done through pixel-wise matching and Fourier transform. Once the instants are obtained, both images are exhibited in the three dimensional space so that we can evaluate the quality of the registration. The presented results show that the time discretization does not allows good results.*

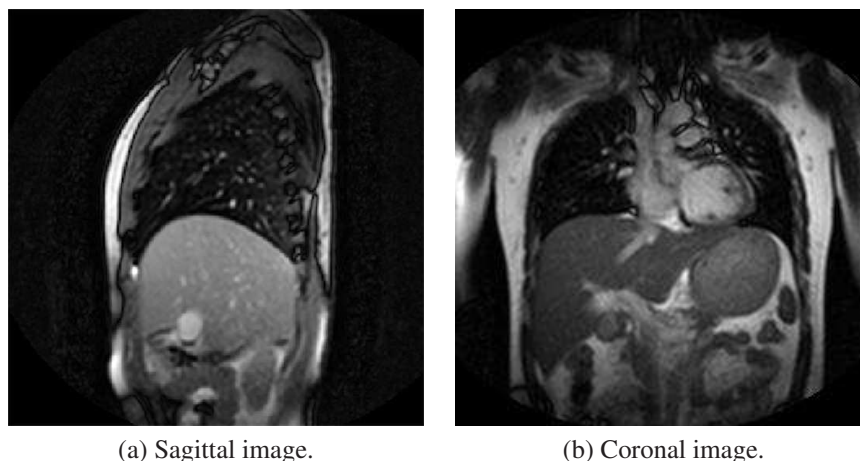
**Keywords:** *Magnetic Resonance Imaging; Lung Reconstruction; Image Processing*

### 1. INTRODUCTION

The three dimensional reconstruction of the lung for visualization purposes is still an open issue in medicine. Images of internal organs may be generated for several purposes, with the aid of contrast substances, giving support to a vast range of medical analysis. An example is the imaging of the ventilated area of the lung using hyperpolarized helium-3 ( $^3\text{He}$ ) gas, an efficient contrast for MR Imaging. If estimates of the total volume of the lung and the ventilated volume of the lung are available, accurate quantitative functional analysis of the lungs ventilation may be performed and accurate quantitative analysis of lungs functionality is at the base of precise evaluation of treatments and evolution of respiratory diseases.

Lung deformations have been studied for the verification of medical imaging equipments and for medical training purposes. The initial methods to model the lung deformation were based on physiology and clinical measurements. The deformation of the lung model as a linear model was proposed by Promayon et al. (1997). A non-physically-based method to describe lung deformations was proposed using NURBS surfaces based on imaging data from CT scans of actual patients (Tsui et al., 2000). Zordan et al. (2004) created an anatomical inspired, physically based model of human torso for the visual simulation of respiration. To obtain 3D information about the lung from MRI images the boundaries of the lung in each image should be retrieved. Ray et al. (2003) proposed the segmentation of the image by merging parametric contours within homogeneous image regions. In this work a 4D lung model is retrieved from a sequence of MR images taken from a breathing lung. This is accomplished through the analysis of the respiratory motion of the lung boundaries. DeCarlo et al. (1995) examined the Finite Element Method implementation of a two-dimensional idealized lung.

Physiologically, very little is understood about the respiratory movement. Troyer et al. (2003) exposed the ribs of a dog and fixed some spindles to measure the respiratory movement. This research walks in the direction of a safer and more accurate measurement method. It is possible to examine the respiratory functioning and lung capacity using extremely



(a) Sagittal image.

(b) Coronal image.

Figure 1. Samples of MR images, coronal and sagittal.



Figure 2. Two disjoint intersecting images from the same lung. The mismatch is more evident on the contour of the diaphragmatic surface.

low price and simple devices; however, for patients with bad health condition such devices are useless. Patients that brief with pain must get accustomed with the devices and this is a difficult task. A safer and more accurate evaluation of the respiratory movement will help in the selection of the appropriate medicine, the determination of the effectiveness of a treatment, to reduce the number of cases of clinical trial, observe the progress of rehabilitation treatments, among other possible applications.

The lung presents some characteristics that do not allow a direct observation. The movement of the lung is passive, a result of the movement of other parts of the body, such as the diaphragm and the thoracic cage, and it is not possible to observe the lung directly, as it collapses if the thoracic cage is opened. The use of internal organ imaging devices turned to be the unique path for lung visualization. High-speed X-ray Computerized Tomography systems are under development and allow the visualization of 3D descriptions of internal structures in time. The large field of view of the lung, although, makes the use of those systems prohibitive due to the high radiation exposition. Considering the safety of the subjects under observation, Magnetic Resonance (MR) devices are preferable. On the other hand, MR imaging systems are too slow to generate enough images in a time interval to build a 3D description of a moving organ such as the lung. Independently of the imaging device used, the images obtained from internal organs suffer from some characteristic imperfections, as images are generated in an indirect form, pixel intensities are resultant from volume averaging, resulting in heterogeneous intensities, low resolution and low SNR. The direct consequence of this severe imaging limitation is that often the boundaries of internal organs are not closed, as some parts are not visible, and therefore disconnected. Considering the imaging of the lung using MR devices, those limitations are aggravated. MR devices measure magnetic fields that are directly correlated to the proton density of the matter. As the lung is filled mainly by air, the proton density is low and no image is generated of the inside part of the lung. The quick movement of some structures also affect the polarization, such as the pulsate movement of the fluids inside the vessels. This polarization disturbance affects de imaging of those structures, making them visible only in some time instants.

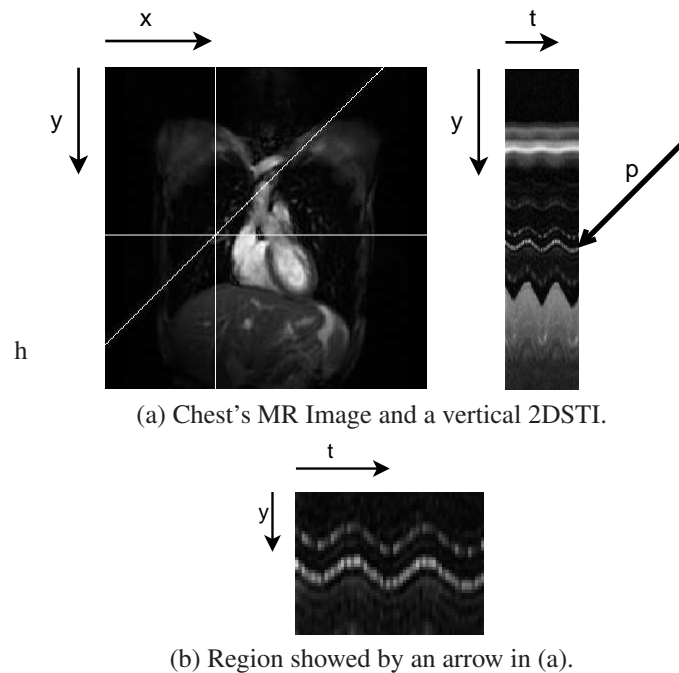


Figure 3. A sample of a chest MR image and its 2D spatio temporal images (2DSTI).

Tsuzuki et al. (2005, 2006, 2007, 2009) and Nakamura et al. (2005) researched the temporal registration of coronal and sagittal vectorial silhouettes of the lung extracted from magnetic resonance images. The lung contour is extracted through different approaches and a polygonal representation for the coronal and sagittal silhouettes are obtained. A wire-frame model of the lung is created by composing the coronal and sagittal planar silhouettes representing cross sections. The polygonal registration happens in the three dimensional space. The wire-frame model is meshed defining a B-Rep solid model. However, the registration based exclusively on vectorial information is not trustable, mainly because it is very hard to verify and confirm the results. The information present in the images is redundant and should be used in the registration. A pixel in a magnetic resonance image can be mapped to the three dimensional space easily by using the DICOM mapping matrix (Tsuzuki et al., 2009), however this matrix is not invertible. This way, a three dimensional point in the space can not be mapped to the magnetic resonance image. This work solves this problem by defining a pseudo inverse knowing in advance that the three dimensional point lies on the magnetic resonance image. The intersection between sagittal and coronal images is a line segment that is determined on each image sequence. The registration is implemented using two different approaches, the first approach analyzes pixel by pixel and the second approach uses Fourier Transform. Finally, some results are presented.

## 2. Problem Statement

Figure 1.(a) shows an example of MR sagittal image and Fig. 1.(b) shows a coronal image. These two images were taken in different instants of time. Accurate three-dimensional description of internal organs may be generated using surface based approaches for the segmentation of a stack of images - a volumetric intensity map of this organ. Those voxel based descriptions may be generated from a set of MR images only for non-moving and non-deforming internal structures, as the MR imaging process is slow and the construction of this volumetric description must happen in a slice-to-slice based registration process. In the case of the lung, a three dimensional volumetric description can not be built through the use of both a large set of MR images and a good registration method, because each image of each slice is taken in a different time instant, with the lung at different stages of the inflating/deflating process. This situation is illustrated in Fig. 2 where two disjointed intersecting images (coronal and sagittal) of the lung are shown.

Consider two temporal sequences of images a coronal and sagittal - one for each type. Fig. 3.(a) shows a temporal sequence of coronal images, with the first coronal image of the sequence on the left and a temporal image on the right. The horizontal axis represents time and the vertical axis represents space. The movement of chest and its internal organs is captured in the temporal space image. Fig. 3.(b) shows an ampliation of Fig. 3.(a). The curve shown in Fig. 3.(b) is dotted, showing the influence of the heart beating in the imaging.

The objective of this research is to find the best image in a coronal sequence that fits to a given sagittal image, and vice-versa. This way it is possible to visualize the chest three dimensionally, by composing all images in the sequence.

Table 1. DICOM data for the sagittal and coronal images used in this work

|            | sagittal | coronal |
|------------|----------|---------|
| $x_x$      | 0.0      | 1.0     |
| $x_y$      | 1.0      | 0.0     |
| $x_z$      | 0.0      | 0.0     |
| $y_x$      | 0.0      | 0.0     |
| $y_y$      | 0.0      | 0.0     |
| $y_z$      | -1.0     | -1.0    |
| $\Delta_i$ | 1.48     | 1.64    |
| $\Delta_j$ | 1.48     | 1.64    |
| $s_x$      | -60.0    | -205.7  |
| $s_y$      | -211.0   | 5.0     |
| $s_z$      | 191.5    | 215.7   |

### 3. Coronal DICOM to Sagittal DICOM Pixel Mapping

The pixels contained in a DICOM image can be mapped to the three dimensional space according to the following

$$\begin{bmatrix} p_x \\ p_y \\ p_z \\ 1.0 \end{bmatrix} = \begin{bmatrix} x_x \cdot \Delta_i & y_x \cdot \Delta_j & 0.0 & s_x \\ x_y \cdot \Delta_i & y_y \cdot \Delta_j & 0.0 & s_y \\ x_z \cdot \Delta_i & y_z \cdot \Delta_j & 0.0 & s_z \\ 0.0 & 0.0 & 0.0 & 1.0 \end{bmatrix} \cdot \begin{bmatrix} i \\ j \\ 0.0 \\ 1.0 \end{bmatrix} = [M] \cdot \begin{bmatrix} i \\ j \\ 0.0 \\ 1.0 \end{bmatrix} \quad (1)$$

where  $i$  and  $j$  are the column and row to the image plane.  $x_x, x_y$  and  $x_z$  are the row  $x$  direction cosine of the image orientation.  $y_x, y_y$  and  $y_z$  are the column  $y$  direction cosine of the image orientation.  $\Delta_i$  is the column pixel resolution and  $\Delta_j$  is the row pixel resolution.  $s_x, s_y$  and  $s_z$  are the start position for the first voxel. Usually, coronal images have a bigger value for  $\Delta_i$  and  $\Delta_j$  when compared to sagittal images from the same patient.

#### 3.1 The Common Line Segment

The sagittal image and the coronal image have a common line segment in the three dimensional space. This common line segment must be analyzed in the definition of the fitting algorithm. We are interested in a set of pixels from the coronal and sagittal images that occupies the same three dimensional space

$$P_s = [M_s] \cdot \begin{bmatrix} i_s \\ j_s \\ 0 \\ 1 \end{bmatrix} = [M_c] \cdot \begin{bmatrix} i_c \\ j_c \\ 0 \\ 1 \end{bmatrix} = P_c \quad (2)$$

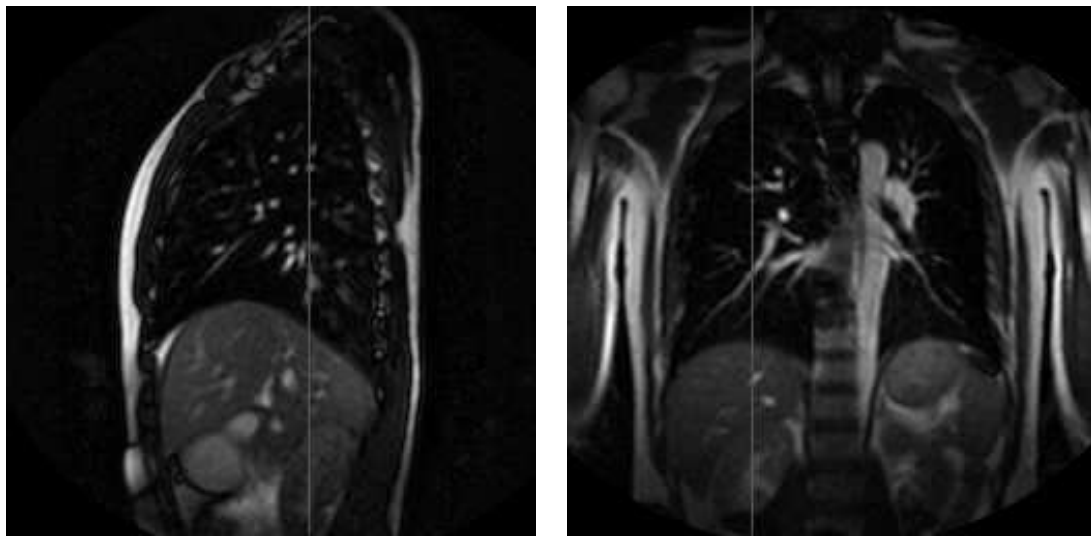
where  $[M_s]$  and  $[M_c]$  are, respectively, the sagittal and coronal mapping matrix. It is possible to isolate one of the two dimensional coordinates

$$\begin{bmatrix} i_s \\ j_s \\ 0 \\ 1 \end{bmatrix} = [M_s]^{-1} \cdot [M_c] \cdot \begin{bmatrix} i_c \\ j_c \\ 0 \\ 1 \end{bmatrix} \quad (3)$$

The parameters of the acquired images are described according to Table 1. Substituting the values from Table 1 in Equation (3) the mapping matrix for sagittal and coronal images are respectively obtained

$$[M_s] = \begin{bmatrix} 0.0 & 0.0 & 0.0 & -60.0 \\ 1.48 & 0.0 & 0.0 & -211.0 \\ 0.0 & -1.48 & 0.0 & 191.5 \\ 0.0 & 0.0 & 0.0 & 1.0 \end{bmatrix} \quad (4)$$

$$[M_c] = \begin{bmatrix} 1.64 & 0.0 & 0.0 & -205.7 \\ 0.0 & 0.0 & 0.0 & 5.0 \\ 0.0 & -1.64 & 0.0 & 215.7 \\ 0.0 & 0.0 & 0.0 & 1.0 \end{bmatrix} \quad (5)$$



(a) Sagittal image.

(b) Coronal image.

Figure 4. The common line segment shown in the sagittal and coronal images. The common vertical line segment is placed at  $i_c = 89$  (coronal image) and  $i_s = 146$  (sagittal image).

### 3.2 The Inverse Matrix

Matrix  $[M]$  shown in equation ( 1) has no inverse, as it has a column filled with zeros. Another information that must be observed is the fact that in the two dimensional space, the coordinate  $z$  has no meaning and can be considered as void. This way, it is possible to modify the values of the third column allowing it to have an inverse. Equations ( 4) and ( 5) are modified according to the following

$$[M_s^*] = \begin{bmatrix} 0.0 & 0.0 & 1.0 & -60.0 \\ 1.48 & 0.0 & 0.0 & -211.0 \\ 0.0 & -1.48 & 0.0 & 191.5 \\ 0.0 & 0.0 & 0.0 & 1.0 \end{bmatrix} \quad (6)$$

$$[M_c^*] = \begin{bmatrix} 1.64 & 0.0 & 0.0 & -205.7 \\ 0.0 & 0.0 & 1.0 & 5.0 \\ 0.0 & -1.64 & 0.0 & 215.7 \\ 0.0 & 0.0 & 0.0 & 1.0 \end{bmatrix} \cdot \quad (7)$$

Now, equations ( 2) and ( 3) becomes

$$P_s = [M_s^*] \cdot \begin{bmatrix} i_s \\ j_s \\ 0 \\ 1 \end{bmatrix} = [M_c^*] \cdot \begin{bmatrix} i_c \\ j_c \\ 0 \\ 1 \end{bmatrix} = P_c \implies \begin{bmatrix} i_s \\ j_s \\ 0 \\ 1 \end{bmatrix} = [M_s^*]^{-1} \cdot [M_c^*] \cdot \begin{bmatrix} i_c \\ j_c \\ 0 \\ 1 \end{bmatrix} \quad (8)$$

where

$$[M_s^*]^{-1} = \begin{bmatrix} 0.0 & 0.67 & 0.0 & 142.6 \\ 0.0 & 0.0 & -0.67 & 129.4 \\ 1.0 & 0.0 & 0.0 & 60.0 \\ 0.0 & 0.0 & 0.0 & 1.0 \end{bmatrix} \quad (9)$$

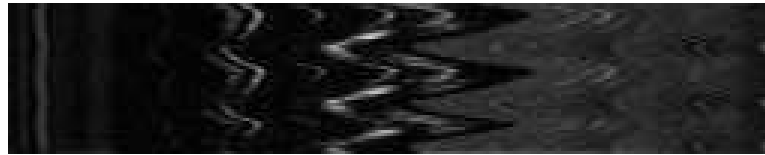
$$[M_c^*]^{-1} = \begin{bmatrix} 0.61 & 0.0 & 0.0 & 125.4 \\ 0.0 & 0.0 & -0.61 & 131.5 \\ 0.0 & 1.0 & 0.0 & -5.0 \\ 0.0 & 0.0 & 0.0 & 1.0 \end{bmatrix} \cdot \quad (10)$$

### 3.3 Common Line Segment Shown in the Image

Now it is possible to determine which pixels from the coronal image are in the sagittal image and vice-versa. Consider the following matrix multiplication:



(a) Coronal sequence.



(b) Sagittal sequence.



(c) Coronal cropped sequence.

Figure 5. The common line segment in time: (a) coronal, (b) sagittal and (c) coronal cropped images.

$$[M_c^*]^{-1} \cdot [M_s] = \begin{bmatrix} 0.0 & 0.0 & 0.61 & 88.8 \\ 0.0 & 0.90 & 0.0 & 14.7 \\ 1.48 & 0.0 & 0.0 & -216.0 \\ 0.0 & 0.0 & 0.0 & 1.0 \end{bmatrix} \quad (11)$$

$$[M_s^*]^{-1} \cdot [M_c] = \begin{bmatrix} 0.0 & 0.0 & 0.67 & 145.5 \\ 0.0 & 1.10 & 0.0 & -15.1 \\ 1.64 & 0.0 & 0.0 & -145.7 \\ 0.0 & 0.0 & 0.0 & 1.0 \end{bmatrix} \quad (12)$$

The final mapping is shown below

$$\begin{bmatrix} i_c \\ j_c \\ dummy \\ 1.0 \end{bmatrix} = \begin{bmatrix} 88.8 \\ 14.7 + 0.90 \cdot j_s \\ -216.0 + 1.48 \cdot i_s \\ 1.0 \end{bmatrix} \quad (13)$$

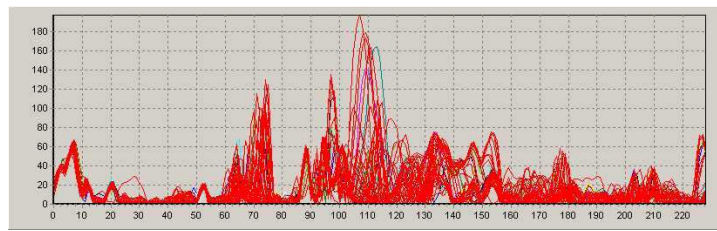
$$\begin{bmatrix} i_s \\ j_s \\ dummy \\ 1.0 \end{bmatrix} = \begin{bmatrix} 145.9 \\ -15.1 + 1.10 \cdot j_c \\ -145.7 + 1.64 \cdot i_c \\ 1.0 \end{bmatrix} \quad (14)$$

As a consequence the sagittal images are contained in the same  $i_c = 88.8$  coordinate and vice-versa ( $i_s = 145.9$ ). Both images have 256 pixels, but the pixels from the sagittal images ( $\Delta_{sj} = 1.48$ ) have a smaller dimension when compared to the pixels from the coronal images ( $\Delta_{cj} = 1.64$ ). Fig. 4 shows the common line segment in the sagittal and coronal images.

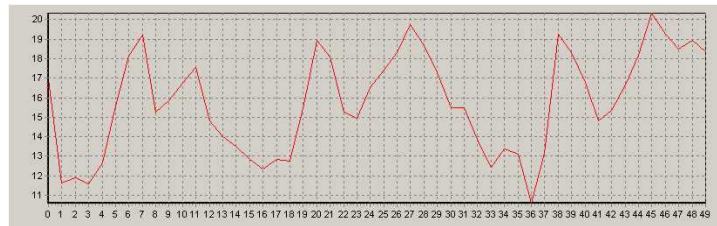
Consider the 2 dimensional space time image for the sagittal and coronal sequences obtained at  $i_c = 89$  (coronal image) and  $i_s = 146$  (sagittal image). Figs. 5.(a) and 5.(b) show these images. The coronal image must be cropped between pixels 15 and 244 (Fig. 5.(c) shows the coronal cropped image).

#### 4. The Registration Algorithm

We have two images representing the same object but viewed from different angles and positions. There are several approaches to measure the similarity between two images, in this particular problem it is searched the similarity between two one dimensional images. Basically these approaches determine the distance between the images by comparing pixel by pixel and combining these differences in a single value. The comparison algorithm should be chosen according to the a priori known information about the acquisition process and the expected image degradation. Two approaches are presented in this work: pixel by pixel comparison and Fourier Transform based.

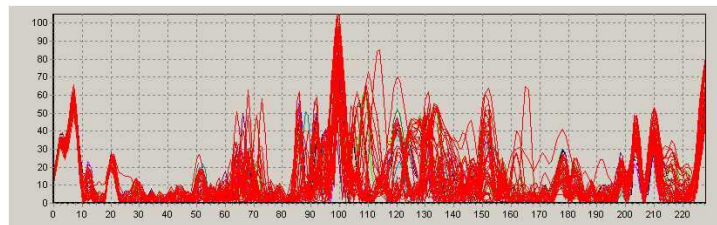


(a) Graphs for all 50 sagittal images and their pixel distance compared to the 7-th coronal image.

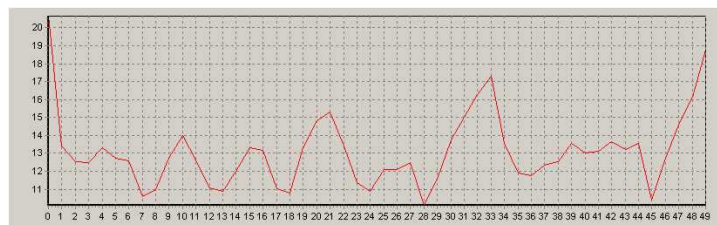


(b) Total distance for all 50 sagittal images when compared to the 7-th coronal image.

Figure 6. Graphs showing the distance of every sagittal image in the temporal sequence ad the 7-th coronal image.



(a) Graphs for all 50 coronal images and their pixel distance compared to the 36-th sagittal image.



(b) Total distance for all 50 coronal images when compared to the 36-th sagittal image.

Figure 7. Graphs showing the distance of every coronal image in the temporal sequence ad the 36-th sagittal image.

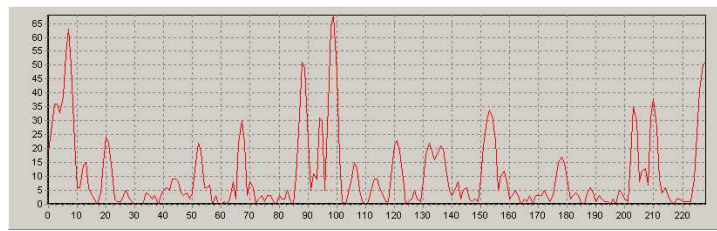
#### 4.1 Pixel by Pixel Comparison

Defining that the two given images 5.(b) and 5.(c) are respectively denoted by  $I_s(t_s, y)$  and  $I_c(t_c, y)$ . Then the register can be defined by the following

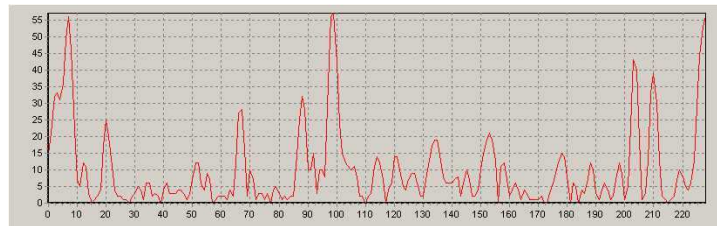
$$e = \sum_y^n \|I_s(t_s, y) - I_c(t_c, y)\|/n \quad (15)$$

where  $e$  is the distance between the two one dimensional images and  $n$  is the number of pixels. The algorithm searches for, given a sagittal image, the coronal image that minimizes the value of  $e$ , and vice-versa. Fig. 6.(a) shows the distance between each pixel from the intersection of all sagittal images and the 7-th coronal image. Coordinate  $y$  ranges from 0 to 229 and there are 50 sagittal images. The main difference is situated between pixels 60 and 190. Fig. 6.(b) shows the totalization graph for all 50 sagittal images and the best registration happens with the sagittal image 36.

In the following example, it happens the opposite, for a given coronal image the algorithm searches for the best sagittal image in the sequence that minimizes the value of  $e$ . Fig. 7.(a) shows the distance between each pixel from the intersection of all coronal images and the 36-th sagittal image. Fig. 7.(b) shows the totalization graph for all 50 coronal images and the best registration happens with the sagittal image 28.

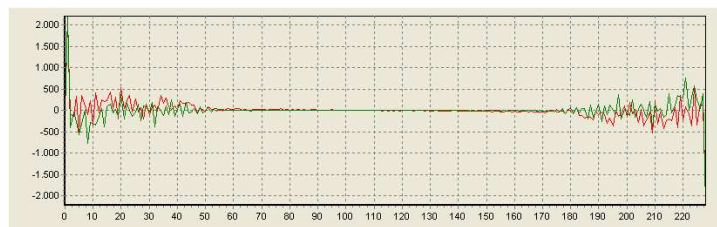


(a) Graph comparing the distance pixel by pixel between the 36-th sagittal image and the 7-th coronal image.

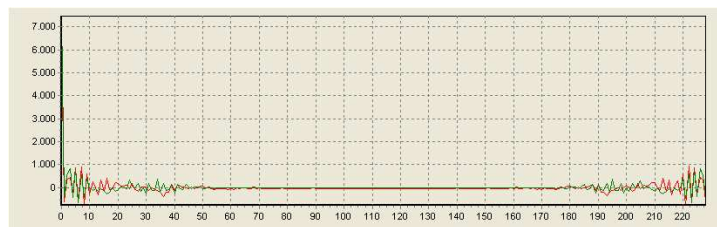


(b) Graph comparing the distance pixel by pixel between the 36-th sagittal image and the 28-th coronal image.

Figure 8. Comparison graphs for coronal images 7 and 28 with the sagittal image 36.



(a) Graph comparing the Fourier transform real component.



(b) Graph comparing the Fourier transform imaginary component.

Figure 9. Fourier transform comparison graphs for coronal image 7 and sagittal image 36.

The results show that the similarity mapping is not commutative. The 7-th coronal image is more similar to the 36-th sagittal image, however the opposite is not the same. The 36-th sagittal image is more similar to the 28-th coronal image. Figs. 8.(a) and 8.(b) show a graph with the distance pixel by pixel between the 36-th sagittal image and, respectively, the 7-th and 28-th images.

#### 4.2 Fourier Transform Based Registration

The Fourier transform provides information about the global frequency-domain characteristics of an image. The Fourier description can be computed using discrete techniques, which are natural for digital images. The discrete Fourier transform used was the following

$$F(u) = \frac{1}{N} \sum_{x=0}^{N-1} f(x) e^{i2\pi ux/N} \quad (16)$$

for  $u = 0, 1, 2, \dots, N - 1$ . The complex coefficients  $F(u)$  are called as Fourier descriptor. It is possible to drop the Fourier descriptors with higher frequencies because their contribution to the image is very small. Fourier descriptors are often used to smooth out fine details in a shape. Filtering an image with Fourier descriptors provides a simple technique

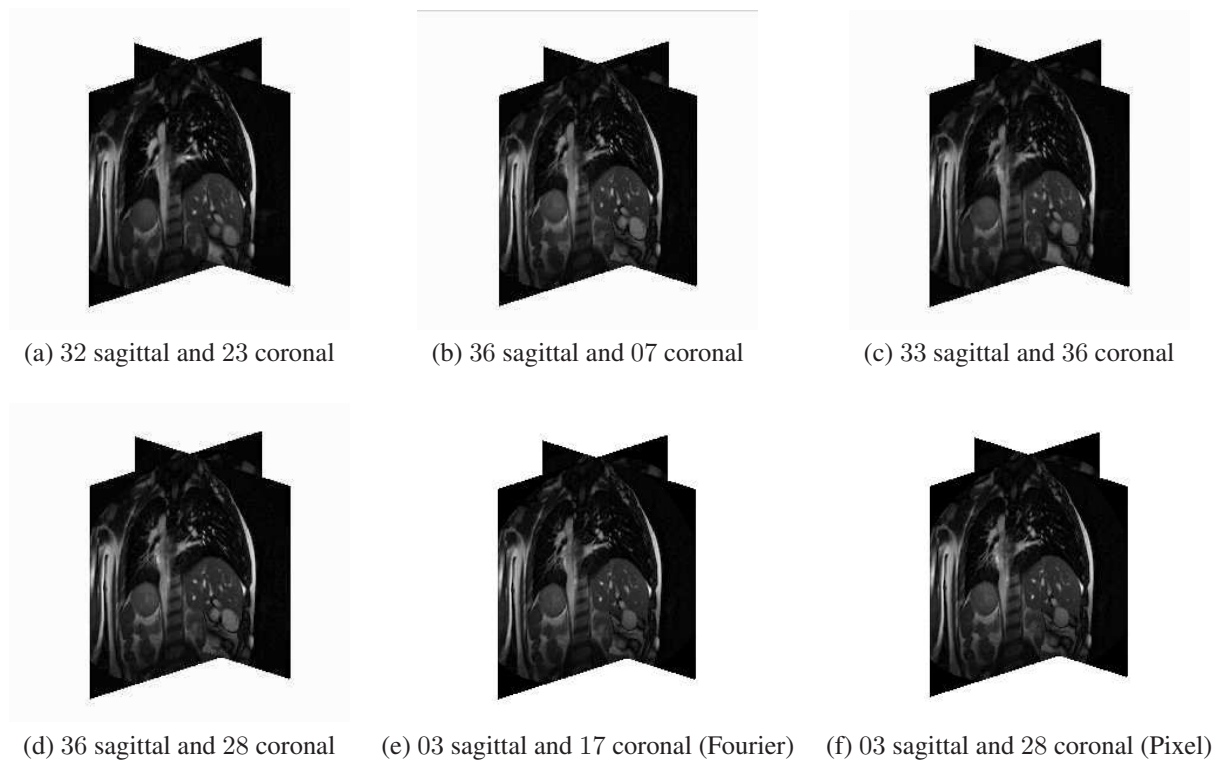


Figure 10. (a)-(d) Samples of registered sagittal and coronal images whose results coincided with both methods. (e)-(f) Samples of registered pairs where both algorithms had different results.

of contour smoothing. Fourier description of an edge is also used for template matching. Since all the Fourier descriptors except the first  $F(0)$  do not depend on the location of the edge within the segment (Gonzalez and Woods, 1993; Russ, 1992; Sonka et al., 1993; Weeks, 1996). The images shown in Fig. 5.(b) and 5.(c) were used directly in this proposal. The number of pixels in the vertical of both images is different, but the real size is the same. It was considered a discretization of the real size and the registration was defined by the following

$$e_f = \sum_u^N \|F_s(u) - F_c(u)\| \quad (17)$$

where  $F_s(u)$  and  $F_c(u)$  are the sagittal and coronal Fourier descriptors, respectively. Figs. 9.(a) and 9.(b) show the graph comparing, respectively, the Fourier transform real and imaginary components between coronal image 7 and sagittal image 36.

## 5. Results and Discussion

When coronal and sagittal images are put together, it is possible to make a visual evaluation of the results. Figs 10.(a)-(d) show examples of the registration algorithm (both algorithms showed the same results in these specific cases). In other situations, the two algorithms resulted with different pairs. Figs 10.(e)-(f) show examples where the resulting pairs from both algorithm are different. It is important to notice that both pairs have a satisfactory visual registration. The temporal sequence of images represent discrete instants in time, and such an almost perfect fitting as shown in Figs. 10.(a)-(f) is very rare. In case the acquisition could happen in a much faster speed, such that the movement of the lung and adjacent organs will be captured with much more details, then registration based exclusively on pixel comparison can be a good approach.

A better approach can be a combination of pixel comparison and time segmentation algorithms. Matsushita et al. (2004) proposed a time segmentation based on the determination of the respiratory movement (see Fig. 3) and Hough transform. This time segmentation algorithm was improved by Tavares et al. (2009) by applying interval arithmetics. Asakura et al. (2005) proposed an algorithm to determine the movement of a pixel synchronously to the respiratory movement. Time segmentation algorithms can support an almost continuous registration. However, it is not reliable to make time registration exclusively on time segmentation algorithms because it is not possible to verify and confirm the results.

## 6. Conclusions

The DICOM mapping matrix was successfully inverted by using an artifice. The temporal registration algorithm based on pixel by pixel comparison and Fourier transform showed several satisfactory results, however it is not possible to overcome the temporal low rate of image acquisition. This preliminary work defined a research direction, one of the future works is the definition of a new registration algorithm combining pixel comparison and time segmentation.

## 7. ACKNOWLEDGEMENTS

Marcos de Sales Guerra Tsuzuki was partially supported by the CNPq. This research was supported by FAPESP.

## 8. REFERENCES

- Asakura, A., Gotoh, T., Kagei, S., Iwasawa, T., Inoue, T., 2005, "Computer Aided System for Respiratory Motion Analysis of the Lung Region by Sequential MR Images.", *Medical Imaging Technology*, v. 23, n. 1, pp. 39–46.
- DeCarlo, D., Kaye, J., Metaxas, D., Clarke, J. R., Webber, B., Badler, N., 1995, "Integrating Anatomy and Physiology for Behavior Modeling.", *Medicine Meets Virtual Reality 3*, San Diego.
- Gonzalez, R.C., Woods, R.E., 1993, *Digital Image Processing*, Addison-Wesley Publishing Company.
- Matsushita, K., Asakura, A., Kagei, S., Gotoh, T., Iwasawa, T., Inoue, T., 2004, "Shape Tracking on Chest MR Sequence Images Using Respiratory Patterns", *Journal of Electronic Imaging*, v. 33, n. 6, pp. 1115–1122.
- Nakamura, C., Asakura, A., Tsuzuki, M.S.G., Gotoh, T., Kagei, S., Iwasawa, T., 2005, "Three Dimensional Lung Modeling from Sequential MR Images Based on Respiratory Motion Analysis". *IEICE Technical Report*, v. 105, pp. 33-38.
- Promayon, E., Baconnier, P., Puech, C., 1997, "Physically-Based Model for Simulating the Human Trunk Respiration Movements.", In *Lecture notes in Computer Science*, Springer Verlag, CVRME II-MRCAS III first joint conference, v. 1205, pp. 379–388.
- Ray, N., Acton, S. T., Altes, T., de Lange, E. E., Brookeman, J. R., 2003, "Merging Parametric Active Contours Within Homogeneous Image Regions for MRI-Based Lung Segmentation.", *IEEE Transactions on Medical Imaging*, v.22, n. 2, pp.189–199.
- Russ, J.C., 1992, *The Image Processing Handbook*, CRC Press.
- Sonka, M., Hlavac, V., Boyle, R., 1993, *Image Processing: Analysis and Machine Vision*, Chapman and Hall.
- Takase, F.K., Tsuzuki, M.S.G., Gotoh, T., Kagei, S., Asakura, A., Iwasawa, T., 2007, "4D Modeling of the Lung by Registering Orthogonal Unsynchronized MR Images". *Proceedings of the COBEM 2007 - 19th International Congress of Mechanical Engineering*, Brasília, Brazil.
- Tavares, R.S., Tsuzuki, M.S.G., Gotoh, T., Kagei, S., Iwasawa, T., 2009, "Lung Movement Determination in Temporal Sequences of MR Images Using Hough Transform and Interval Arithmetics". *Proceedings of the 7th IFAC Symposium on Modelling and Control in Biomedical Systems*, Aalborg, Denmark.
- Troyer, A. D. and Leduc, D., 2003, "Effects of Inflation on the Coupling Between the Ribs and the Lung in Dogs.", *J. Physiol.*, v. 555, n. 2, pp. 481–488.
- Tsui, B. M. W., Segars, W. P., Lalush, D. S., 2000, "Effects of Upward Creep and Respiratory Motion in Myocardial SPECT.", *IEEE Transactions on Nuclear Science*, v. 47, pp. 1192-1195.
- Tsuzuki, M.S.G., Takase, F.K., Asakura, A., Gotoh, T., Kagei, S., Iwasawa, T., 2005, "4D Thoracic Organ Modelling from Unsynchronized MR Sequential Images". *Proceedings of the 12th ICBME - 12th International Conference on Biomedical Engineering*, Singapore, Singapore.
- Tsuzuki, M.S.G., Takase, F.K., Asakura, A., Gotoh, T., Kagei, S., Iwasawa, T., 2006, "Visualization of a 4D B-Rep Solid Model of the Lung Constructed from Unsynchronized MR Sequential Images". *Proceedings of the 12th International Conference on Geometry and Graphics*, Salvador, Brazil.
- Tsuzuki, M.S.G., Takase, F.K., Asakura, A., Gotoh, T., Kagei, S., Iwasawa, T., Inoue, T., 2009, "Animated Solid Model of the Lung Constructed from Unsynchronized MR Sequential Images". *Computer Aided Design*, v. 41, pp. 573–585.
- Weeks Jr, A., 1996, *Fundamentals of Electronic Image Processing*, IEEE Press.
- Zordan, V. B., Celly, B., Chiu, B., DiLorenzo, P. C., 2004, "Breathe Easy: Model and Control of Simulated Respiration for Animation.", *Proceedings of the 2004 ACM SIGGRAPH/Eurographics symposium on Computer animation 2004*, Grenoble, France.

## 9. Responsibility notice

The author(s) is (are) the only responsible for the printed material included in this paper